DATA REPOSITORY ITEM

We revised the slip rate of the Pisgah fault by remapping and dating the dextrally offset Lavic basalt flow. Hart et al. (1988) reported dextral displacement of this flow by 600 to 800 m and estimated its age at 900 ka from correlation of its weathered surface to other dated lava flows in the Mojave Desert. Using high-resolution air photos acquired after the 1999 Hector Mine earthquake, we remapped pyroclastic deposits capped by the Lavic flow that are dextrally displaced 725±85 m by fault slip (Figure DR1). Though the offset locality lies within a restricted portion of a military base, we were able to acquire a sample of the Lavic flow for $^{40}Ar/^{39}Ar$ geochronology. Basalt glass groundmass was separated from phenocrysts and analyzed by the furnace incremental heating method following procedures in Singer et al. (2004). The age spectra from the Lavic flow are discordant such that increments which define a contiguous age plateau at the 95% confidence level give apparent ages significantly younger than adjacent increments (Table DR2, Figure DR2). These results therefore strongly suggest that extraneous argon is present, either due to older material incorporated into the magma en route to the surface, or the presence of excess argon in the magma at the time of eruption. The spectra step down from apparent ages of nearly 4 Ma at low temperature to plateau ages of about 1100 ka that comprise 80-95% of the gas released. The MSWD (York, 1969) values for these age plateaus are slightly larger than expected due to inclusion of steps near 60% of the ^{36}Ar released that have relatively low K/Ca ratios and slightly higher ages (Table DR2). The isochron age of 752 ± 110 ka, which makes no assumption about the initial composition of argon in the system, gives the best estimate of time since this lava was erupted. Based on this new age and our revised mapping we determine a maximum slip rate of 1.0±0.2 mm/yr for the Pisgah fault (Table 1), which is slightly higher than the ~0.8 mm/yr reported by Hart et al. (1988) due to a younger than estimated age of the Lavic basalt flow.

Renne, P.R., Swisher, C.C.I., Deino, A.L., Karner, D.B., Owens, T.L., and DePaolo, D.J., 1998, Intercalibration of standards, absolute ages and uncertainties in $^{40}Ar/^{39}Ar$ dating: Chemical Geology, v. 145, p. 117-152.

Singer, B.S., Ackert, R.P., and Guillou, H., 2004, $^{40}Ar/^{39}Ar$ and K-Ar chronology of Pleistocene glaciations in Patagonia: Geological Society of America Bulletin, v. 116, p. 434-450.

Steiger, R.H., and Jager, E., 1977, Subcommision on geochronology: Convention on the use of decay constants in geo- and cosmochronology: Earth and Planetary Science Letters, v. 36.

York, D., 1969, Least squares fitting of a straight line with correlated errors: Earth and Planetary Letters, v. 5, p. 320-324.

Figure DR1. Interpreted air photo map of pyroclastic deposits (shaded red) dextrally offset 725 ± 85 m by slip on the Pisgah fault. Steep dip angle of basalt-pyroclastic deposits contact supports that these deposits were probably emplaced as a cinder cone across the trace of the fault. Because the Lavic basalt flow overlies these deposits, this offset is a maximum value for offset of the lava flow. Contact relationships of the Lavic basalt to the undivided basalt and cinder cone are uncertain but do not affect the offset result.

Figure DR2. Apparent age spectra and K/Ca release pattern (left) and inverse isochron diagram (right) for replicate analyses of samples of the Lavic basalt flow. Portions of the spectra that yielded age plateaus are shown by the arrows. Only these plateau data are combined to calculate the isochron ages shown at the right (data from individual experiments normalized to a common J value for illustrative purposes only). Combining the regressions of these 22 plateau steps yields an isochron age of 752±110 ka and indicates that the lava contains argon with an initial $^{40}Ar/^{36}Ar$ ratio of 303.4 ± 2.5 which is significantly higher than the value of 295.5 for the atmosphere.

Figure DR3. Top: Preferred, minimum, and maximum restorations of slip on the Ludlow fault determined from offset of walls of channel A. Bottom: Annotated field photograph of study site taken from locality shown by yellow star on map at upper left. This photograph shows geologically mapped location of the Ludlow fault and nearby inactive faults that separate volcaniclastic conglomerate from andesite breccia and ash deposits. Key marker of fault slip is channel A that lies inset below thin $Q2_a$ alluvial terrace deposit. For offset of 19 ± 4 m it is assumed that this channel crossed the active Ludlow fault at a right angle when incision of the $Q2_a$ terrace deposit commenced. The offset and slip rate could be reduced if there was an initial right-jog in the stream channel along the fault prior to incision of $Q2_a$. Restoration of greater than 23 m of offset is unlikely, as this would place a steep ridge of volcaniclastic conglomerate in front of channel A.

Figure DR4. Top: Minimum and maximum restorations of slip on the Camp fault determined from reconstruction of displaced remnants of $Q2_a$ alluvial fan. Bottom: Annotated field photograph of study site taken from locality shown by yellow star on map at upper left. This photograph shows parts of $Q2_a$ fan that have been displaced by dextral Camp Rock fault slip. Bedrock east of fault is quartz monzonite. Shutter ridge west of fault is quartz monzonite breccia shed from across the fault. Volcanic clasts derived from headwaters of channel B uniquely tie $Q2_a$ fan remnants to this sediment source. Due to uncertainty of extent of $Q2_a$ fan east of fault, between 20 to 70 m of dextral slip may be restored to align this fan with its continuation west of the fault. The maximum offset of 70 m places the $Q2_a$ fan east of the fault immediately opposite of the channel leading to the $Q2_a$ fan west of the fault. Significantly less offset would be required if channel B was deflected around the shutter ridge during deposition of $Q2_a$.

Figure DR5. Top: Preferred, minimum, and maximum restorations of slip on the Lenwood fault determined from offset of walls of channels C and D. Bottom: Annotated field photograph of study site taken from locality shown by yellow star on map at upper left. This photograph shows location of the Lenwood fault mapped on the basis of well-defined topographic scarp. Here the fault juxtaposes similar outcrops of early Miocene conglomerate. Steep-walled canyons of channels C and D are inset below $Q2_b$ alluvial fans downstream of the fault. Thus the offset of these channels is interpreted to have commenced after abandonment of the $Q2_b$. Shown in the photograph is the offset of the south wall of channel D. Topographic data also shows well-defined walls of channel C that are offset by a similar amount. Together, these deflected channels yield a preferred offset of 29 m, with a maximum of 34 m and minimum of 19 m.

Figure DR6. Top: Minimum and maximum restorations of slip on the Helendale fault determined from reconstruction of channels and floodplain inset below $Q2_b$ alluvial fan. Bottom: Annotated field photograph of study site taken from locality shown by yellow star on map at upper left. This photograph shows cosmogenic ^{10}Be sample pit with anomalously thick argillic soil horizon. Helendale fault forms scarp in bedrock in the background. Maximum slip restores floodplain E as a linear feature crossing the trace of the Helendale fault. This restoration also aligns smaller channels F and G. Minimum slip is estimated by projecting the incised edge of the $Q2_b$ alluvial fan to the corresponding wall of channel E southwest of the fault. The maximum offset of 45 m was used to derive a conservative upper bound on the Helendale fault slip rate.

DR2008119

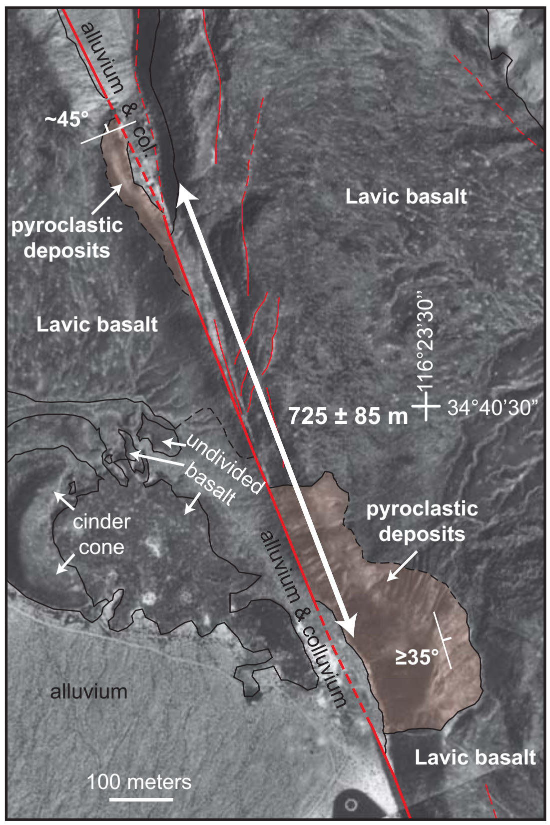

alluvium & col
~45°
pyroclastic deposits
Lavic basalt
Lavic basalt
116°23'30"
725 ± 85 m
34°40'30"
undivided basalt
cinder cone
alluvium & colluvium
pyroclastic deposits
≥35°
alluvium
Lavic basalt
100 meters

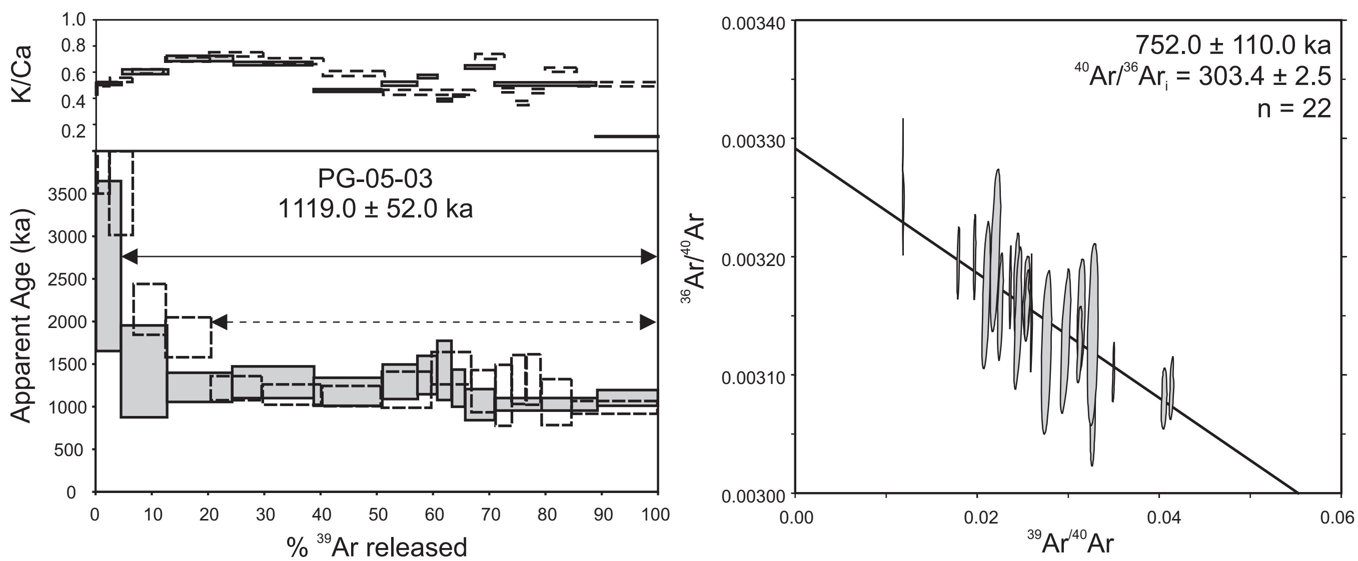
K/Ca
PG-05-03
1119.0 ± 52.0 ka
Apparent Age (ka)
% 39Ar released
752.0 ± 110.0 ka
40Ar/36Ari = 303.4 ± 2.5
n = 22
36Ar/40Ar
39Ar/40Ar

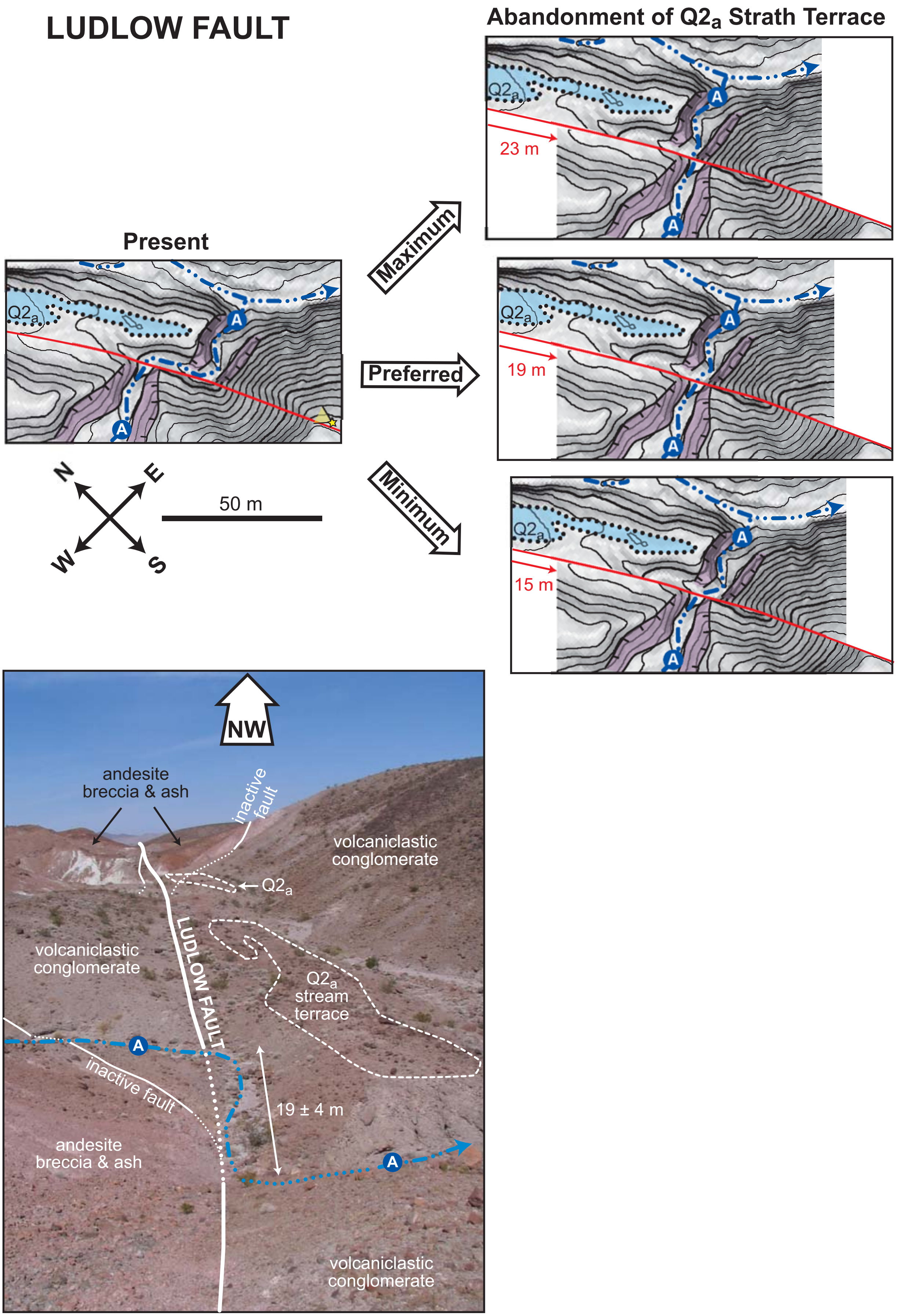
LUDLOW FAULT
Abandonment of Q2a Strath Terrace
Present
Q2a
A
Maximum
Preferred
Minimum
23 m
19 m
15 m
N
E
W
S
50 m
NW
andesite
breccia & ash
inactive
fault
volcaniclastic
conglomerate
Q2a
LUDLOW FAULT
Q2a
stream
terrace
inactive fault
19 ± 4 m
andesite
breccia & ash
volcaniclastic
conglomerate

DR2008119

CAMP ROCK FAULT

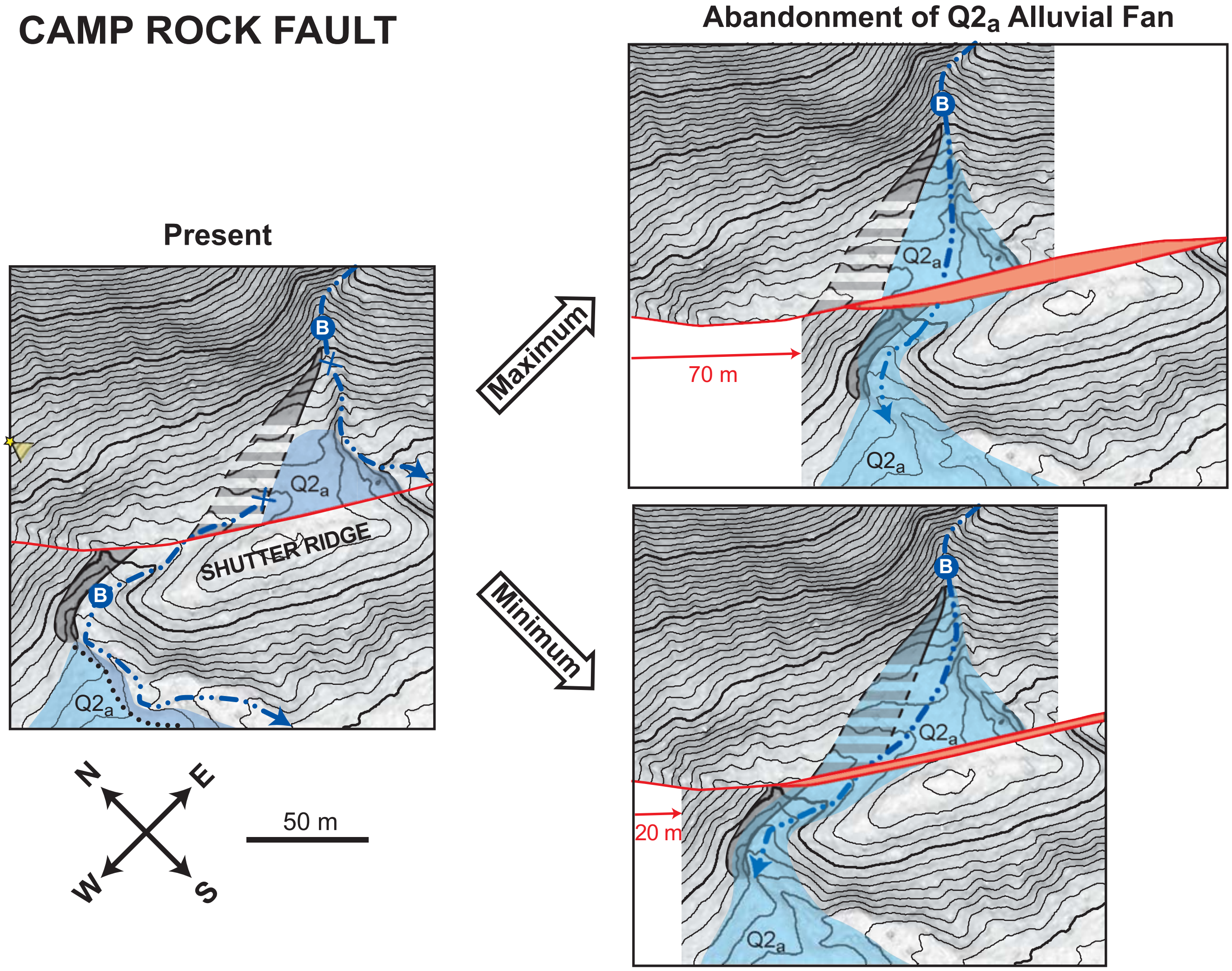

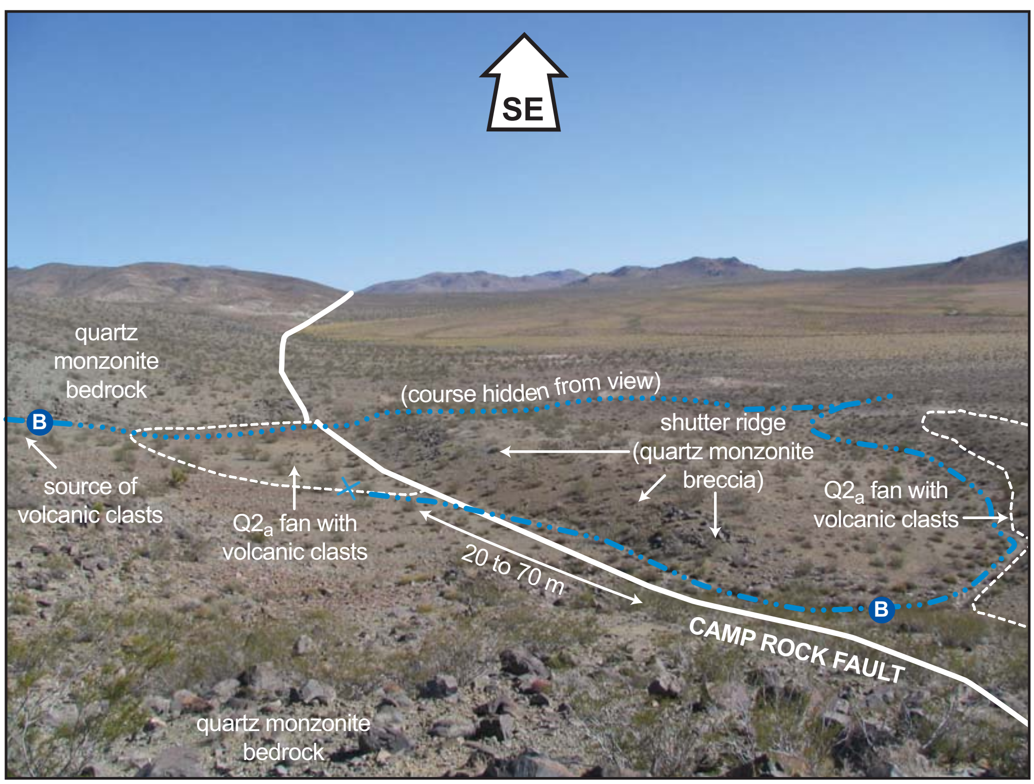

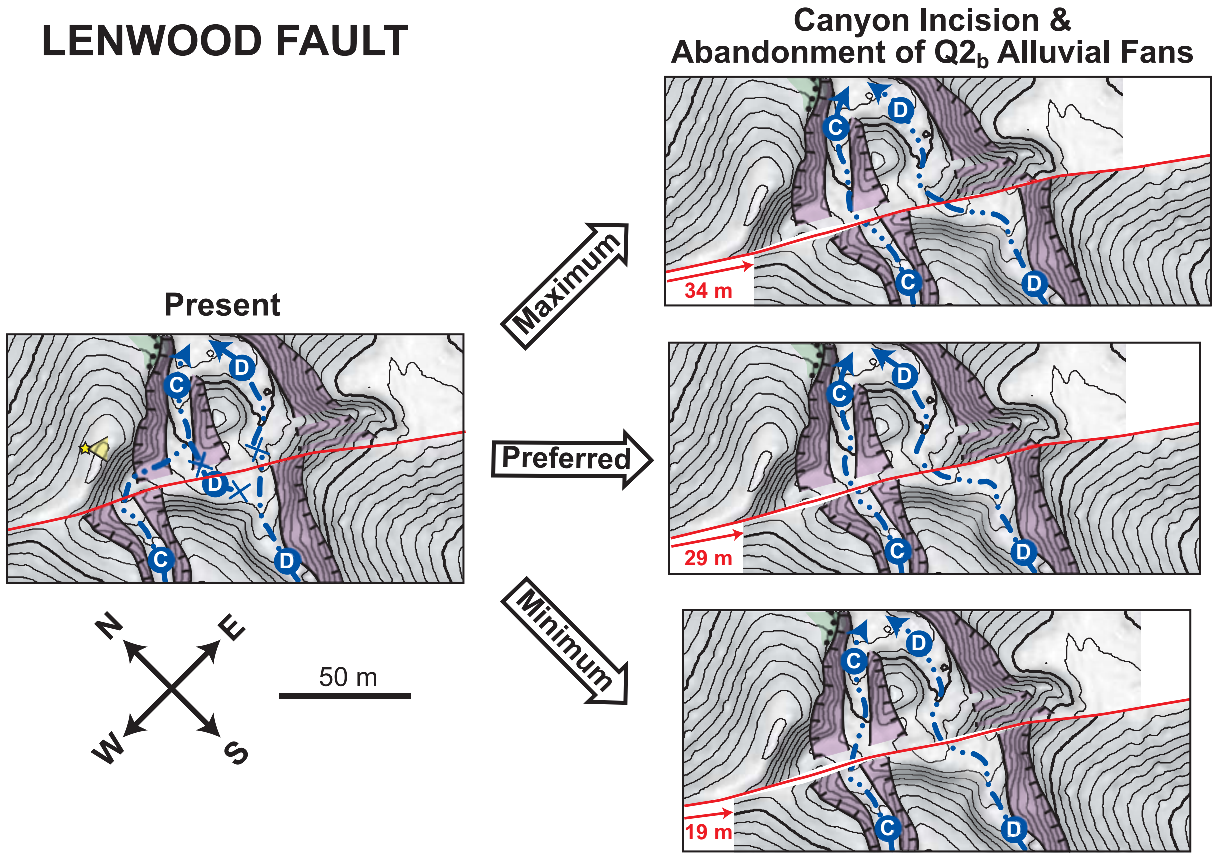
LENWOOD FAULT
Canyon Incision & Abandonment of Q2b Alluvial Fans
Present
Maximum
Preferred
Minimum
34 m
29 m
19 m
C
D
N
E
W
S
50 m


SE
29 +5/-10 m
channel wall
channel wall
D
D
C
C
LENWOOD FAULT

HELENDALE FAULT

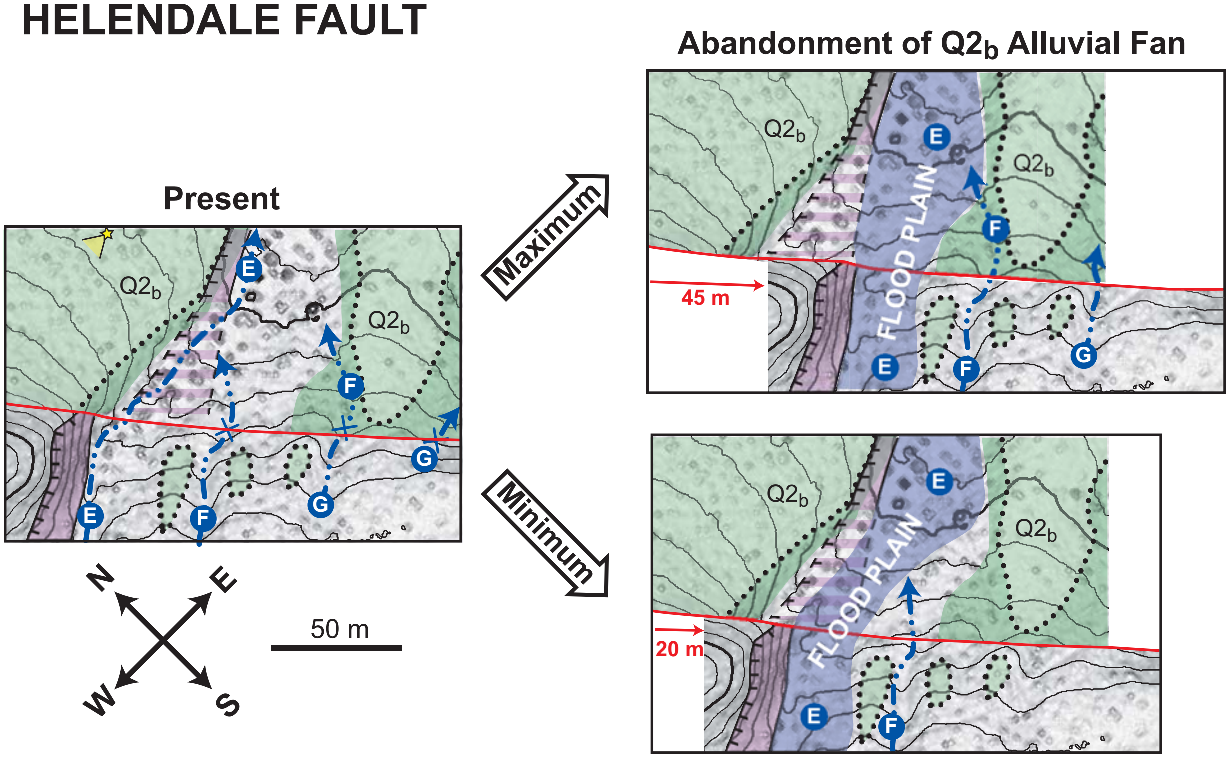

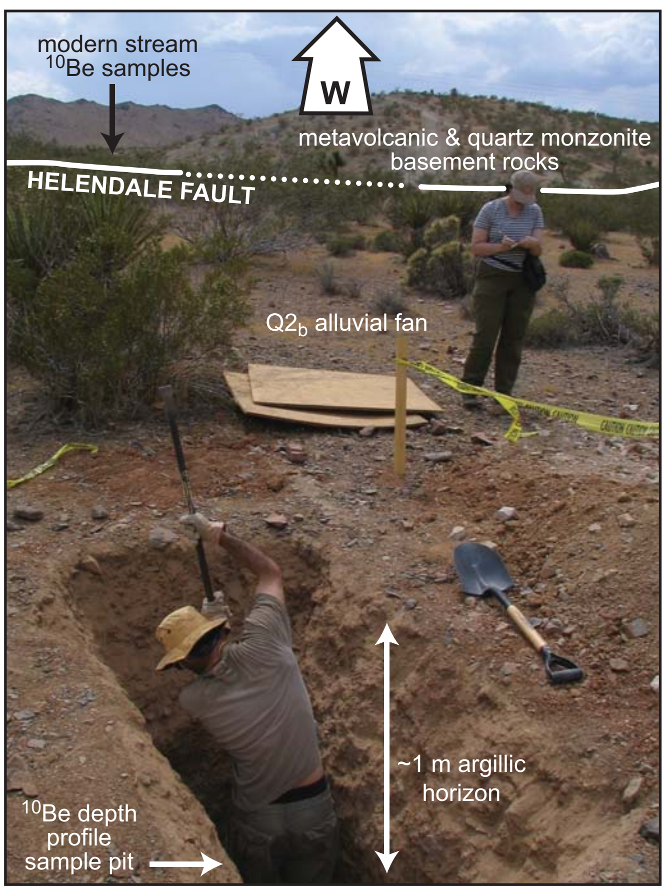

Table DR1. Cosmogenic ^{10}Be Analyses

Locality	Sample #	Grain size	Depth (cm)	$^{10}Be/^{9}Be$ ratio ($\times10^{-12}$)	Atoms/g quartz ($\times10^{5}$)		
Lenwood Q2b fan, 34.7433°N, 116.9222°W, 985m					**P_0**	**=**	**9.9**
	LW05-001	pebble	0	3.21	10.05	±	0.26
	LW05-003	pebble	32.5	1.47	8.21	±	0.20
	LW05-004	pebble	75	1.92	7.41	±	0.18
	LW05-005	pebble	135	1.19	7.35	±	0.37
	LW05-008	Sand	135	1.78	8.23	±	0.38
	LW05-009	Sand	75	3.39	8.93	±	0.21
	LW05-010	Sand	32.5	3.21	10.14	±	0.24
	LW05-011	Sand	6	2.18	11.21	±	0.27
	LW05-012	Sand	0	2.77	10.90	±	0.26
Lenwood modern stream, 34.7389°N, 116.9207°W, 1002m							
	LW05-024	pebble	0	3.10	5.97	±	0.14
	LW05-025	Sand	0	1.12	4.17	±	0.19
Helendale Q2b fan, 34.6425°N, 117.1630°W, 1004m					**P_0**	**=**	**10.0**
	HD05-01	mixed	0	2.53	10.11	±	0.27
	HD06-01A	mixed	0	2.63	10.78	±	0.36
	HD06-01	mixed	185	1.22	4.74	±	0.18
	HD06-02	mixed	95	1.50	9.22	±	0.35
	HD06-03	mixed	55	1.38	9.03	±	0.59
	HD06-04	mixed	22.5	1.35	9.47	±	0.34
	HD06-05	mixed	11	1.70	10.43	±	0.35
Helendale modern stream, 34.6425°N, 116.1675°W, 1020m							
	HD06-13	mixed	0	0.84	5.46	±	0.40
	HD06-14	mixed	0	0.51	4.50	±	0.34
Camp Rock Q2a fan, 34.7077°N,116.7544°W, 1140m					**P_0**	**=**	**11.1**
	CR05-01	pebble	0	4.51	18.14	±	1.20
	CR05-02	pebble	0	3.69	14.68	±	0.35
	CR05-03	pebble	0	2.43	8.63	±	0.34
Camp Rock modern stream,34.7092°N, 116.7519°W, 1165m							
	CR06-01	pebble	0	2.24	6.00	±	3.07

Sample targets were prepared at the University of Minnesota with standard mineral separation, etching, dissolution, and purification techniques. Local ^{10}Be production rates, P_0, are calculated with 5.1±0.3 atom/g/yr high-latitude sea level production rate, scaled for latitude and air pressure with 15°C average sea-level temperature (Stone, 2000).

TABLE DR2. $^{40}Ar/^{39}Ar$ INCREMENTAL HEATING RESULTS

PG-05-03 (116.3866°W, 34.6680°N)

101 mg aliquot — Groundmass — J= 0.000260 ± 0.46 % (1σ) — μ = 1.0069 ± 0.05 % (1σ)

ID #		Temp (°C)	$^{40}Ar/^{39}Ar$ ± 1σ	$^{38}Ar/^{39}Ar$ ± 1σ	$^{37}Ar/^{39}Ar$ ± 1σ	$^{36}Ar/^{39}Ar$ ± 1σ	F ± 1σ	$^{39}Ar_k$ (%)	$^{40}Ar^*$ (%)	K/Ca	Apparent Age ± 2σ ka
BD1724		620 °C	1467.8680 ± 17.8925	0.9528 ± 0.0118	1.9025 ± 0.0353	4.9103 ± 0.0594	17.0609 ± 8.0060	0.14	1.16	0.226	7984.9 ± 7477.4
BD1725		670 °C	211.4845 ± 0.8960	0.1444 ± 0.0011	1.6710 ± 0.0178	0.6970 ± 0.0043	5.6452 ± 1.0737	4.59	2.67	0.257	2646.0 ± 1005.8
BD1726	#	720 °C	81.7689 ± 0.2317	0.0627 ± 0.0004	1.4236 ± 0.0150	0.2669 ± 0.0020	3.0288 ± 0.5726	7.92	3.70	0.302	1420.1 ± 536.7
BD1727	#	770 °C	41.9945 ± 0.1420	0.0380 ± 0.0004	1.2163 ± 0.0131	0.1336 ± 0.0006	2.6076 ± 0.1809	11.66	6.20	0.353	1222.7 ± 169.6
BD1728	#	820 °C	30.2445 ± 0.1373	0.0294 ± 0.0003	1.2935 ± 0.0138	0.0934 ± 0.0007	2.7437 ± 0.2023	14.22	9.06	0.332	1286.5 ± 189.6
BD1729	#	870 °C	38.9010 ± 0.1802	0.0347 ± 0.0003	1.8604 ± 0.0205	0.1236 ± 0.0007	2.5195 ± 0.1672	12.21	6.47	0.231	1181.4 ± 156.8
BD1730	#	920 °C	50.0609 ± 0.2295	0.0427 ± 0.0003	1.6765 ± 0.0182	0.1606 ± 0.0008	2.7325 ± 0.2209	6.49	5.45	0.256	1281.3 ± 207.1
BD1731	#	980 °C	43.7635 ± 0.1862	0.0393 ± 0.0003	1.5198 ± 0.0180	0.1386 ± 0.0007	2.9290 ± 0.2464	3.54	6.69	0.283	1373.4 ± 231.0
BD1732	#	1040 °C	47.4285 ± 0.4396	0.0411 ± 0.0006	2.1872 ± 0.0301	0.1508 ± 0.0013	3.0381 ± 0.3719	2.56	6.40	0.196	1424.5 ± 348.7
BD1733	#	1100 °C	38.0669 ± 0.1117	0.0364 ± 0.0006	2.0474 ± 0.0227	0.1206 ± 0.0008	2.6090 ± 0.2323	2.28	6.84	0.210	1223.4 ± 217.8
BD1734	#	1160 °C	31.5349 ± 0.1807	0.0320 ± 0.0003	1.3343 ± 0.0150	0.0997 ± 0.0007	2.1784 ± 0.1850	5.25	6.90	0.322	1021.5 ± 173.4
BD1735	#	1220 °C	24.5057 ± 0.0811	0.0278 ± 0.0003	1.6887 ± 0.0175	0.0759 ± 0.0003	2.2021 ± 0.0771	17.99	8.98	0.254	1032.6 ± 72.3
BD1736	#	1280 °C	28.2737 ± 0.0765	0.0309 ± 0.0002	8.0284 ± 0.0803	0.0899 ± 0.0003	2.3647 ± 0.0895	11.15	8.32	0.053	1108.8 ± 83.9

Total Fusion Age: 1274.2 ± 75.8 — ^{39}Ar % in Plateau 95.3

Weighted Plateau from 11 of 13 Analyses: MSWD 2.47 — Plateau Temp Range 720 °C - 1280 °C — Age: **1126.2 ± 68.2**

Inverse Isochron from 11 of 13 Analyses: MSWD 0.9 — $^{40}Ar/^{36}Ar$ ± 2σ 302.1 ± 3.3 — Age: **820.5 152.2**

115 mg aliquot — Groundmass — J= 0.000260 ± 0.46 % (1σ) — μ = 1.0069 ± 0.05 % (1σ)

ID #		Temp (°C)	$^{40}Ar/^{39}Ar$ ± 1σ	$^{38}Ar/^{39}Ar$ ± 1σ	$^{37}Ar/^{39}Ar$ ± 1σ	$^{36}Ar/^{39}Ar$ ± 1σ	F ± 1σ	$^{39}Ar_k$ (%)	$^{40}Ar^*$ (%)	K/Ca	Apparent Age ± 2σ ka
BD2020		620 °C	2268.5253 ± 40.6423	1.4446 ± 0.0291	1.7372 ± 0.0661	7.4238 ± 0.1298	75.0327 ± 20.3833	0.07	3.30	0.247	34855.9 ± 18756.0
BD2021		650 °C	355.4137 ± 2.8699	0.2341 ± 0.0034	1.7024 ± 0.0296	1.1658 ± 0.0089	11.0634 ± 1.7922	2.21	3.11	0.252	5182.0 ± 1676.5
BD2022		680 °C	166.0960 ± 0.6642	0.1173 ± 0.0010	1.6010 ± 0.0234	0.5341 ± 0.0037	8.4079 ± 0.9872	4.03	5.06	0.268	3939.5 ± 924.1
BD2023		710 °C	91.2583 ± 0.4138	0.0695 ± 0.0007	1.4192 ± 0.0211	0.2938 ± 0.0017	4.5617 ± 0.3348	5.79	4.99	0.303	2138.5 ± 313.7
BD2024		740 °C	55.5408 ± 0.1274	0.0453 ± 0.0008	1.2404 ± 0.0173	0.1752 ± 0.0009	3.8715 ± 0.2543	8.08	6.96	0.346	1815.1 ± 238.3
BD2025	#	770 °C	38.8278 ± 0.1840	0.0345 ± 0.0002	1.1788 ± 0.0166	0.1230 ± 0.0006	2.5870 ± 0.1479	9.26	6.66	0.364	1213.0 ± 138.6
BD2026	#	800 °C	31.6981 ± 0.1523	0.0311 ± 0.0002	1.2631 ± 0.0185	0.0994 ± 0.0005	2.4203 ± 0.1299	10.56	7.63	0.340	1134.9 ± 121.8
BD2027	#	830 °C	30.2428 ± 0.1017	0.0301 ± 0.0003	1.4792 ± 0.0206	0.0948 ± 0.0005	2.3622 ± 0.1269	10.69	7.80	0.290	1107.7 ± 119.0
BD2028	#	860 °C	40.7246 ± 0.1675	0.0370 ± 0.0003	1.9967 ± 0.0278	0.1298 ± 0.0008	2.5287 ± 0.2268	9.05	6.20	0.215	1185.7 ± 212.7
BD2029	#	900 °C	55.2280 ± 0.2348	0.0464 ± 0.0003	1.9146 ± 0.0266	0.1770 ± 0.0008	3.0913 ± 0.2094	7.14	5.59	0.224	1449.4 ± 196.3
BD2030	#	950 °C	33.3422 ± 0.2969	0.0316 ± 0.0004	1.2067 ± 0.0190	0.1046 ± 0.0008	2.5170 ± 0.2586	4.28	7.54	0.356	1180.3 ± 242.5
BD2031	#	1000 °C	45.2205 ± 0.4692	0.0403 ± 0.0005	1.8653 ± 0.0313	0.1454 ± 0.0013	2.3944 ± 0.3889	2.73	5.29	0.230	1122.8 ± 364.6
BD2032	#	1060 °C	40.2596 ± 0.3818	0.0374 ± 0.0005	2.3444 ± 0.0388	0.1274 ± 0.0010	2.8084 ± 0.3085	2.60	6.96	0.183	1316.8 ± 289.2
BD2033	#	1120 °C	35.9742 ± 0.3323	0.0357 ± 0.0005	1.9051 ± 0.0308	0.1127 ± 0.0011	2.8198 ± 0.3117	2.73	7.83	0.225	1322.2 ± 292.2
BD2034	#	1170 °C	30.2476 ± 0.2040	0.0313 ± 0.0003	1.3934 ± 0.0214	0.0952 ± 0.0010	2.2350 ± 0.2858	5.53	7.38	0.308	1048.0 ± 267.9
BD2035	#	1220 °C	23.9814 ± 0.0726	0.0271 ± 0.0002	1.6942 ± 0.0235	0.0745 ± 0.0003	2.0939 ± 0.0794	15.23	8.72	0.253	981.9 ± 74.4

Total Fusion Age: 1490.7 ± 74.8 — ^{39}Ar % in Plateau 79.8

Weighted Plateau from 11 of 16 Analyses: MSWD 3.14 — Plateau Temp Range 770 °C - 1220 °C — Age: **1109.2 ± 81.5**

Inverse Isochron from 11 of 16 Analyses: MSWD 0.39 — $^{40}Ar/^{36}Ar$ ± 2σ 305.1 ± 3.7 — Age: **665.0 171.9**

All ages calculated relative to 1.194 Ma for the Alder Creek rhyolite sanidine (Renne et al., 1998) using the decay constants of Steiger and Jäger (1977).

reactor constants are as follows: $[^{40}Ar/^{39}Ar]_K$ = 0.00086; $[^{36}Ar/^{37}Ar]_{Ca}$ = 0.000264; $[^{39}Ar/^{37}Ar]_{Ca}$ = 0.000673.

^{37}Ar and ^{39}Ar corrected for post-irradiation decay, half lives of 35.2 days and 269 years, respectively

\# indicates increments that have been included in weighted plateau and isochron calculations

$^{38}Ar/^{39}Ar$ ratio is not corrected for background signal